

Fluid-structure interaction and its effect on the performance of composite structures under air-blast loading

Erheng Wang¹, Nate Gardner², Sachin Gupta² and Arun Shukla^{2,*}

¹Department of Aerospace Engineering, University of Illinois at Urbana-Champaign Urbana, IL, 61801, Email: erhengwang@gmail.com

²Dynamic Photomechanics Laboratory, Department of Mechanical, Industrial and Systems Engineering, University of Rhode Island, Kingston, RI 02881, USA Email: nate.gardner11@gmail.com, gupsac@my.uri.edu

ABSTRACT

Three material systems: E-glass Vinyl-Ester (EVE) composites, sandwich composites with EVE facesheet and monolithic foam core (2 different core thicknesses), and monolithic aluminum alloy plates, were subjected to shock wave loading to study their blast response and fluid-structure interaction behaviors. High-speed photography systems were utilized to obtain the real-time side-view and back face deformation images. A 3-D Digital Image Correlation (DIC) technique was used to analyze the real-time back face displacement fields and subsequently obtain the characteristic fluid-structure interaction time. The reflected pressure profiles and the deflection of the back face center point reveal that the areal density plays an important role in the fluid-structure interaction. The predictions from Taylor's model (classical solution, does not consider the compressibility) and model by Wang *et al.* (considers the compressibility) were compared with the experimental results. These results indicated that the model by Wang *et al.* can predict the experimental results accurately, especially during the characteristic fluid-structure interaction time. Further study revealed that the fluid-structure interaction between the fluid and the sandwich composites cannot be simplified as the fluid-structure interaction between the fluid and the facesheet. Also, it was observed that the core thickness affects the fluid-structure interaction behavior of sandwich composites.

Keywords: Glass-fiber reinforced composites, Sandwich composites, Fluid-structure interaction, 3-D Digital image correlation, Blast loading, Compressibility.

1. INTRODUCTION

The dynamic behavior of composite materials under blast loading is usually separated into two main stages: the fluid-structure interaction stage and the post-failure stage [1, 2]. Though the dynamic behavior of composite materials under blast loading has been studied

*Corresponding author, E-mail: shuklaa@egr.uri.edu, Tel: 401-874-2283, Fax: 401-874-2355

experimentally [1, 3–8], theoretically [2, 7, 9, 10] and numerically [6, 11–14] for decades, most of the work only focuses on the post-failure stage. The fluid-structure interaction stage is still not well understood, especially in a highly compressible fluid, such as air. However, early failure can occur at the fluid-structure interaction stage and significantly affect the post-failure behaviors of sandwich composites. Therefore, understanding the fluid-structure interaction behavior, such as characteristic interaction time, helps in evaluating the blast performance of materials and structures, and consequently guides new designs of novel materials and structures to better mitigate high-intensity blast loadings.

There are two reasons which make it difficult to investigate the fluid-structure interaction during a blast loading: (1) the absence of accurate models, and (2) the limitation of experimental techniques. The classic and most popular theoretical solution for the fluid-structure interaction between a blast pulse and a monolithic plate was developed by Taylor [15]. He combined the one-dimensional linear wave theory with the rigid body motion theory to predict the dynamic pressure applied on the plate. However, this theory does not consider the non-linear compressibility of the fluid, such as air. Therefore, it is only valid for the prediction in an incompressible fluid, such as water [2, 16]. Furthermore, due to the short time period of the blast event, proper measurement techniques are under-developed, especially high-speed visualization techniques, to identify the fluid-structure interaction. Since it is extremely difficult to separate the fluid-structure interaction stage from the post-failure stage and conduct a quantitative investigation, experimental results available in literature on the fluid-structure interaction are extremely limited.

The difficulties in theoretical and experimental aspects also limit the numerical study. Generally, there are two ways to simplify the fluid-structure interaction stage numerically. The first one assumes a uniform velocity field of the solid target at the end of the fluid-structure interaction stage, and utilizes Taylor's model to calculate the target velocity [12, 14]. This velocity field is utilized as the input for the numerical model. The second one directly uses the experimental reflected pressure or force profile as the input for the numerical model [17]. However, both ways have their own limitations. The first way ignores the interaction between the components of composite materials. Therefore, simulated results have been questioned when applied to the study of the blast resistance of sandwich composites [16]. The second way confuses the cause and effect. It is the response of composite materials which causes the reflected pressure or force profile, not the reflected pressure profile which causes the response. Therefore, it is difficult to predict the reflected pressure or force profile without conducting a real experiment for an unknown material. Recently, few studies have been reported that simulate the fluid structure interaction process by coupling fluid and solid elements through Dynamic System Mechanics Analysis Simulation (DYSMAS) software [18].

For this study, we use a new theoretical model, proposed in our former work [13], and a high-speed photography system coupled with 3-D Digital Image Correlation (DIC) technique to investigate the full-field real-time response of composite materials subjected to blast loading. Three material systems were investigated: E-glass Vinyl-Ester (EVE) composites, sandwich composites with EVE facesheet and monolithic foam core (2 different core thicknesses), and monolithic aluminum alloy plates. A shock tube apparatus was utilized to generate approximately identical incident blast overpressures on the specimens. The reflected pressure profiles, along with the full-field back-view deformations and side-view deflections were obtained from the high-speed photography system and DIC technique. The fluid-structure interaction behaviors, such as characteristic interaction time, were analyzed in detail. The experimental results were then compared

with the theoretical predictions, and the differences in the fluid-structure interaction of the different material systems are shown.

2. THE FLUID-STRUCTURE INTERACTION MODELS

Consider a uniform, planar blast wave propagating with a constant velocity, U , in a fluid of density, ρ_f , and impinging normally upon a free-standing flat target, with an areal density, ρ_s . An approximate blast pressure profile is shown in Figure 1. It has a very sharp jump at time $t = 0$ with a very high overpressure in relation to the background pressure (normally the atmospheric pressure). After the sharp jump, the pressure decays very quickly and even goes to a pressure level lower than the background pressure. The time at which the blast pressure is equal to background pressure is defined as positive time period, t_+ . The most common approximation of this pulse is expressed with an exponential decay profile [19–21],

$$p(t) = p_{peak} e^{-\frac{t}{\theta}}, \quad 0 \leq t \leq \infty \tag{1}$$

where, p_{peak} is the peak pressure. θ is the time constant and can be expressed by the positive time period, t_+ and the peak pressure, p_{peak} :

$$\theta = \frac{t_+}{\ln(p_{peak}) - \ln(p_0)} \tag{2}$$

where, p_0 is the background pressure or the base pressure.

Note, throughout this manuscript, the traveling direction of the wave is defined as the positive x direction, $x = 0$ is chosen as the original position of the plate, and the out-of-plane displacement of the plate is defined as $w(t)$.

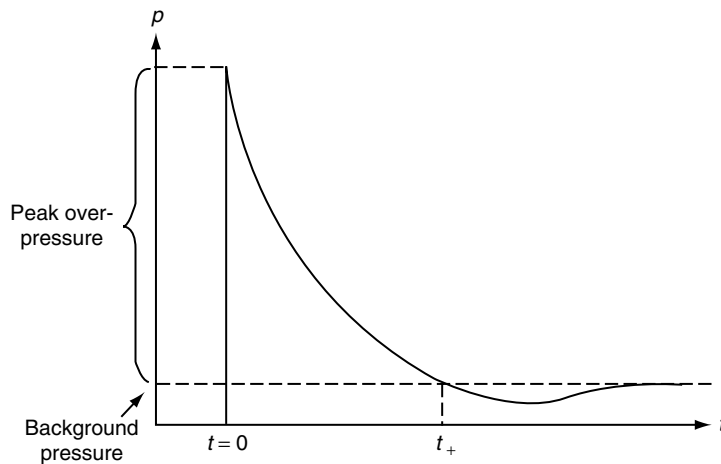


Figure 1 Typical shock pressure profile.

2.1. TAYLOR'S MODEL

In Taylor's model [2, 14, 15], the pressure applied on the plate can be separated into three parts: the pressure of the incoming wave, p_I , the pressure of the reflected wave from a rigid wall, p_{r1} , and the pressure of the rarefaction wave, p_{r2} , due to the acceleration process of the plate. They can be expressed as,

$$p_I(t) = p_{peak} e^{-\left(t - \frac{x}{U}\right)/\theta} \quad (3a)$$

$$p_{r1}(t) = p_{peak} e^{-\left(t + \frac{x}{U}\right)/\theta} \quad (3b)$$

$$p_{r2}(t) = -\rho_f U \dot{w} \left(t + \frac{x}{U} \right) \quad (3c)$$

where, U is the shock wave front velocity. Since the compressibility is ignored, the incident and reflected waves have the same wave front velocity. Therefore, the pressure applied on the plate (at $x = 0$) is,

$$p(t) = p_I(t) + p_{r1}(t) + p_{r2}(t) = 2p_{peak} e^{-\frac{t}{\theta}} - \rho_f U \dot{w}(t) \quad (4)$$

Application of the Newton's second law to the plate results in,

$$\rho_s \ddot{w}(t) = 2p_{peak} e^{-\frac{t}{\theta}} - \rho_f U \dot{w}(t) \quad (5)$$

Considering the initial conditions $w(t) = \dot{w}(t) = 0$ with the understanding that the pressure should approach 0 at the time t_+ , one can obtain the explicit expression of the reflected pressure profile as,

$$p(t) = 2p_{peak} e^{-\frac{t}{\theta}} - \frac{2p_{peak}\psi}{\psi - 1} \left[e^{-\frac{t}{\theta}} - e^{-\frac{\psi t}{\theta}} \right] \quad (6)$$

where $\psi = (\rho_f U \theta) / \rho_s$. The impulse transmitted into the specimen can be calculated as,

$$I_{trans} = \zeta I_{max} \quad (7)$$

where, I_{max} is the maximum achievable impulse that is applied when the wave impinges upon a solid wall, and ζ is the transmitted coefficient. These terms can be expressed as,

$$I_{max} = \int_0^{\infty} 2p_{peak} e^{-\frac{t}{\theta}} dt = 2I_{incident} \tag{8a}$$

$$\zeta = \psi^{-\frac{\psi}{\psi-1}} \tag{8b}$$

2.2. MODEL BY WANG ET AL

In the model by Wang *et al.* [13], the compressibility is considered by utilizing the Rankine-Hugoniot relation of the fluid. The incident pressure (represented by the subscript 1) and reflected pressure (represented by the subscript 2) profiles are all assumed to have a similar expression as that of Eq. (1),

$$p_1(t) = p_{1_peak} e^{-\frac{t}{\theta_1}}, \quad 0 \leq t \leq \infty \tag{9a}$$

$$p_2(t) = p_{2_peak} e^{-\frac{t}{\theta_2}}, \quad 0 \leq t \leq \infty \tag{9b}$$

where, p_{1_peak} and p_{2_peak} are the peak pressures for the incident and reflected pressure pulses, respectively. θ_1 and θ_2 are the time constants for the incident and reflected pressure. Furthermore, assume t_{1+} and t_{2+} are the positive time periods for the incident and reflected pressures which can be related to θ_1 and θ_2 through Eq. (2).

The reflected pressure profile, p_2 , can be calculated from the known incident pressure profile, p_1 , through two steps. The first step is to calculate the peak pressure, p_{2_peak} , of the reflected pressure profile by assuming that the incident shock wave is impinging upon a rigid wall,

$$p_{2_peak} = p_{1_peak} \left\{ \left[\frac{u_{1_peak}}{(1-\mu^2)c_{1_peak}} + \sqrt{\frac{u_{1_peak}^2}{(1-\mu^2)^2 c_{1_peak}^2} + 4} \right]^2 \frac{1+\mu^2}{4} - \mu^2 \right\} \tag{10}$$

where, u_{1_peak} and c_{1_peak} are the peak particle velocity and peak sound velocity of the incident fluid, respectively. They can be calculated using the incident pressure profile. Note, $\mu^2 = \frac{\gamma-1}{\gamma+1}$, where γ is the adiabatic coefficient of the fluid.

The second step is to utilize the conservation of momentum of the plate at the end of the fluid-structure interaction stage,

$$\int_0^{t_+} [p_2(t) - p_0] dt = \rho_s u_2 \Big|_{t=t_+} \quad (11)$$

where, p_0 is the background pressure and ρ_s is the areal density of the target. The reflected particle velocity, u_2 can be calculated from the incident and reflected pressure profiles p_1 and p_2 . Since, p_{2_peak} has been determined in the first step, there is only one unknown parameter (θ_2 or t_+) of the reflected pressure profile, and consequently there is only one unknown parameter in Eq. (11). Therefore, the value of the unknown parameter (θ_2 or t_+) can be obtained by solving Eq. (11). Consequently, all of the other parameters, such as impulse, can be generated using the calculated reflected pressure profile, p_1 , and the known incident pressure profile p_2 . Further details regarding the steps and generation of parameters can be found in Ref. [13].

3. EXPERIMENTAL SETUP

3.1. MATERIALS AND SPECIMENS


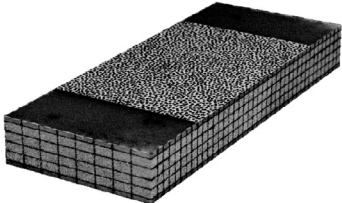
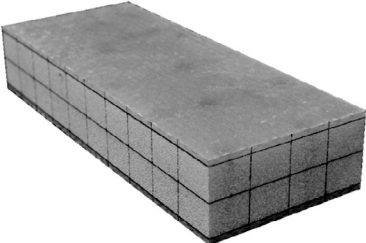
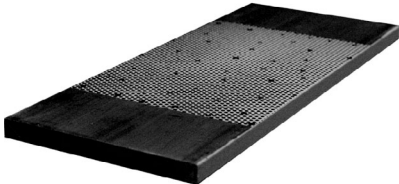
Three different material systems were tested: E-glass Vinyl-Ester (EVE) composites, sandwich composites with EVE facesheet and monolithic foam core (2 different core thicknesses), and monolithic aluminum 6061-T6 alloy plates. The E-glass Vinyl-Ester (EVE) composites utilized 8 layers of woven roving E-glass fibers placed in a quasi-isotropic layout [0/45/90/-45]_s. The fibers were made of the 0.61 kg/m² areal density plain weave. The resin system used was Ashland Derakane Momentum 8084. The EVE composites consisted of identical layup and materials as those used as the front and back facesheets of the two types of sandwich composites in this study. The EVE sandwich composites utilized CoreCell™ P600 foam core. The quasi-static properties of the material systems, as well as their individual components, as obtained from proper ASTM standards (D1621 and D3410) and manufacturer's data [22], are listed in Table 1.

All of the specimens have a cuboid shape approximately 102 mm-wide, 254 mm-long and consist of various thicknesses. The thickness of the EVE composites and facesheets is 3.8 mm. The monolithic foam core of the EVE sandwich composites has two different thicknesses: 25.4 mm and 38.1 mm. The thickness of the aluminum alloy plate is 9.5 mm. Table 2 shows the actual specimens, along with their respective weight and areal density.

Table 1 Material properties of the components.

Material type	Nominal density (kg/m ³)	Compression modulus (GPa)	Compression strength (MPa)	Shear modulus (GPa)
EVE composite	1800	13.6	220	—
P600 foam	122	0.125	1.81	0.056
Al alloy 6061-T6	2700	69	275	26

Table 2 The image, weight and areal density of specimens.

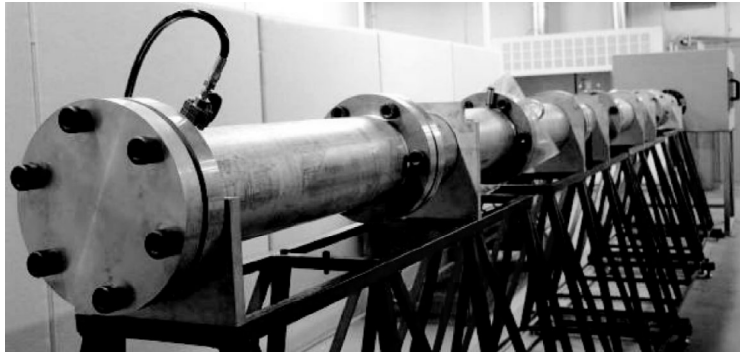
Specimen name	Image	Weight (g)	Areal density (kg/m ³)
EVE composite		177	6.8
Sandwich composite with 25.4 mm monolithic foam core		446	17.2
Sandwich composite with 38.1 mm monolithic foam core		600	23.3
Al alloy 6061-T6		660	25.7

3.2. SHOCK TUBE

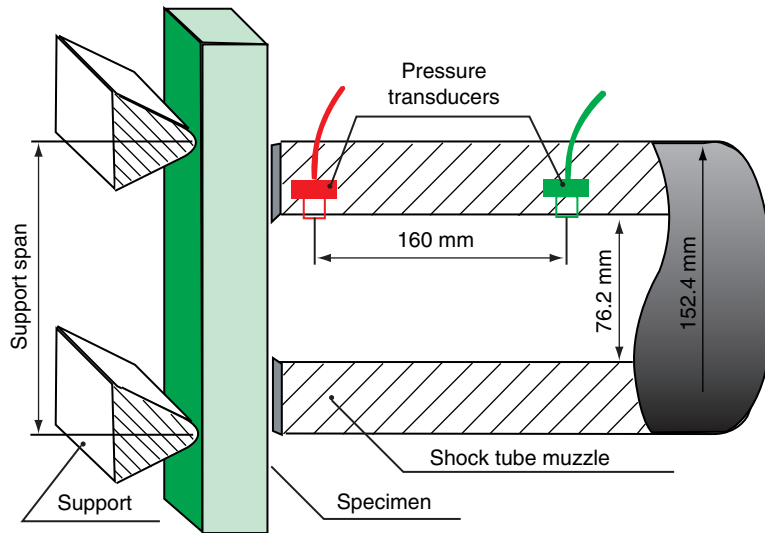
A shock tube apparatus was utilized to obtain a controlled blast loading. The details of this apparatus can be found in Ref. [23]. Figure 2 shows the shock tube apparatus and a detailed view of the muzzle end. The inner diameter of the muzzle is 76.2 mm. Two high frequency response pressure transducers (PCB102A) were mounted at the end of the muzzle section, with a distance of 160 mm between them. The support fixtures ensured simply supported boundary conditions with a 152.4 mm span.

3.3. HIGH-SPEED PHOTOGRAPHY SYSTEMS

Two high-speed photography systems were utilized to capture the real-time 3-D deformation of the specimen. The experimental set-up, as shown in Figure 3, consisted of a back-view 3-D Digital Image Correlation (DIC) system (two cameras) and a side-view camera. The cameras were Photron SA1 digital cameras, and captured the blast event at a framing rate of 20,000 fps with an image resolution of 512 × 512 pixels for a one second time duration. These cameras were synchronized to ensure that the images and data could be correlated and compared.



(a) Shock tube



(b) Dimensions of the muzzle end

Figure 2 Shock tube apparatus.

The 3-D DIC technique is one of the most recent non-contact methods for analyzing full-field shape, motion and deformation. The working mechanism of this technique is similar to how our eyes function. Two cameras capture two images from different angles at the same time. By correlating these two images, one can obtain the three dimensional shape of the surface. Correlating this deformed shape to a reference (zero-load) shape gives full-field in-plane and out-of-plane deformations. The details of this technique can be found in Ref. [24, 25]. In the present study, Vic-3-D DIC software from Correlation Solution, Inc, was utilized to analyze the high-speed images. To ensure good image quality, a speckle pattern with good contrast was placed on the back of the specimen prior to experiments.

3.4. EXPERIMENTAL SET-UP AND PROCEDURE

For each material system, at least three samples were tested to ensure repeatability. The specimens were placed in front of the shock tube muzzle as shown in Figure 2b. The high-speed

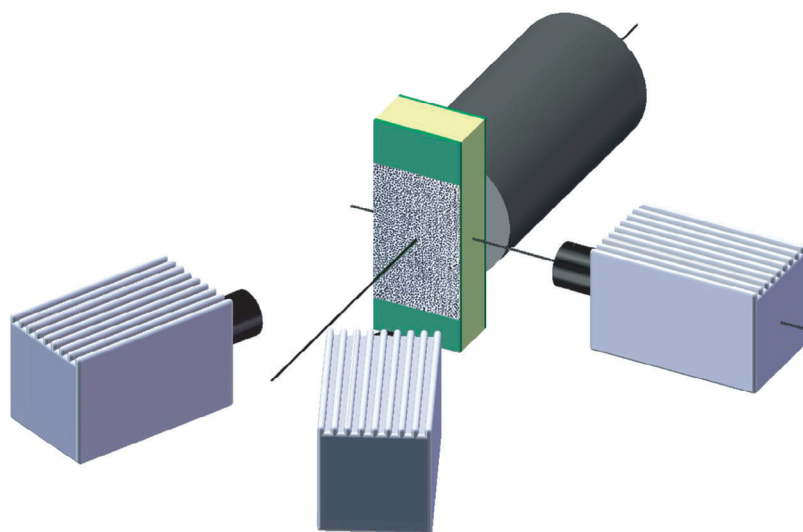


Figure 3 High-speed photography systems.

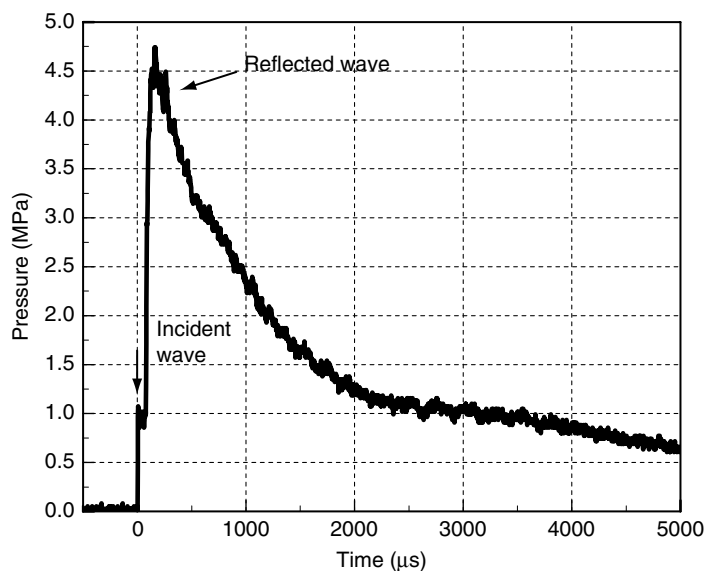


Figure 4 Typical pressure profile from transducer closed to the specimen.

photography systems and the pressure transducers were utilized to capture the deformation images and record the pressure-time history upon the arrival of the shock wave.

A typical pressure profile, as obtained from the transducer closest to the specimen during the shock loading, is shown in Figure 4. It can clearly be seen that there is a low-level incident shock wave with a peak pressure of approximately 1 MPa, followed by a much higher reflected shock wave with a peak pressure of approximately 4.7 MPa. The incident shock wave velocity is approximately 1000 m/s (~Mach 3), while the reflected wave velocity is only 350 m/s (~Mach 1). For a more detailed analysis of the pressure data, refer to Ref. [23].

4. EXPERIMENTAL RESULTS AND DISCUSSION

4.1. REFLECTED PRESSURE PROFILES AND IMPULSES IMPARTED TO THE SPECIMENS

The reflected pressure profiles represent the actual shock load applied on the specimen, which is the result of the fluid-structure interaction. The experimental pressure profiles of the different material systems are plotted in Figure 5. It can be seen that the values of the peak reflected pressure for the different material systems show excellent agreement (< 10% deviation).

The decaying speed of the reflected pressure highly depends upon the material properties. Figure 5 shows that specimens with a higher areal density will decay slower as compared to those of lower areal density. This is due to the fact that a specimen with a higher areal density will achieve a lower velocity under the same blast loading conditions. Therefore, the gas expands less and will maintain a constant applied pressure longer.

The pressure impulse applied on the specimen can be calculated using the follows equation:

$$I_{impulse} = \int_0^t p_2(t) dt \quad (12)$$

The calculated results are shown in Figure 6 and they indicate that the initial fluid-structure interaction behavior only depend on the areal density of the specimens.

4.2. DETERMINATION OF THE CHARACTERISTIC FLUID-STRUCTURE INTERACTION TIME

4.2.1. Core deformations

As discussed by Ref [1, 2], the structural response of a sandwich beam subjected to a blast loading is divided into three (3) sequential steps: stage I is the one-dimensional fluid-structure interaction problem during the blast loading event, in which the front facesheet is

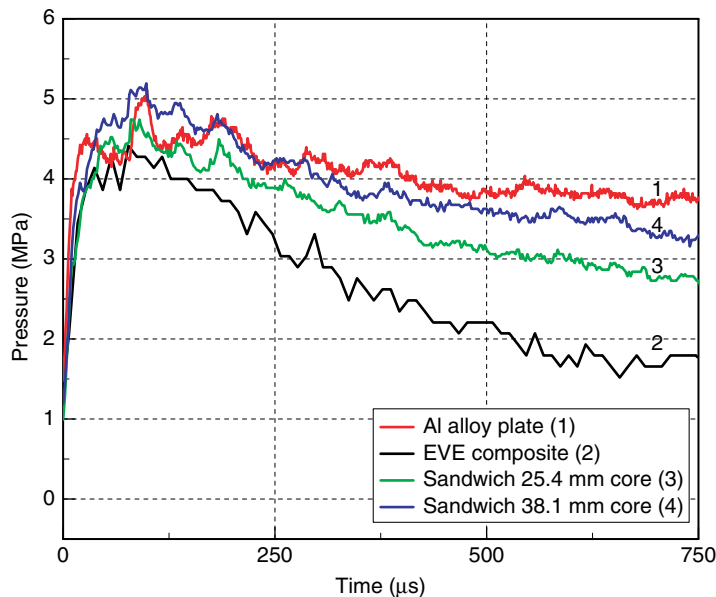


Figure 5 Reflected pressure profiles of different specimens.

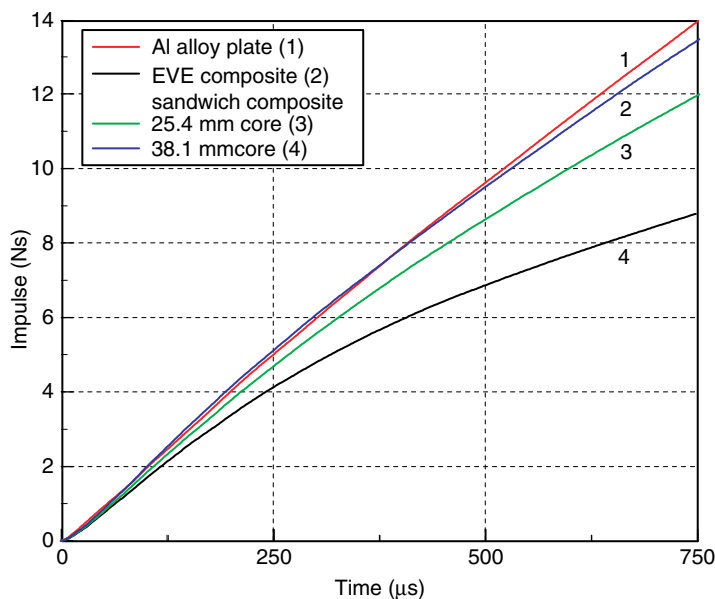


Figure 6 Impulses imparted upon different specimens.

accelerated to a velocity by the incoming shock wave, while the core and the back facesheet remain stationary; during stage II the core compresses and the velocities of the facesheets and core become equalized by momentum sharing; stage III is the retardation phase over which the beam is brought to rest by plastic bending and stretching.

The monolithic plate is too thin for observing the deformation within the thickness. However, the thickness of sandwich composites is enough for applying the 2-D Digital Image Correlation (DIC) technique to obtain the core deformations during the initial shock wave loading. The results of the sandwich composites with a 38.1 mm core are shown here as an example.

The axial strains, e_{xx} , at different locations along the symmetric center-line of the specimen are shown in Figure 7. A contour plot of e_{xx} at time $t = 50 \mu\text{s}$ is also shown on the left side. The shock wave imparts dynamic loading on the specimen from the right side. The facesheet that is in direct contact with the shock wave (blast-receiving side) is called the front face. The face sheet on the opposite side is called the back face.

From the e_{xx} plots on the right side of Figure 7, it can be observed that the axial strain only exhibited a positive value prior to $250 \mu\text{s}$. After $250 \mu\text{s}$, the value of e_{xx} at any point was negative, which indicated that the core was under compression. This turning point on the e_{xx} plot revealed that the deformation mechanism was totally different prior to and after. It also revealed the transition from Stage I (the fluid-structure interaction) to Stage II (core compression) of the deformation process [1, 2]. Therefore, it can be concluded that the characteristic fluid-structure interaction (Stage I) was completed by $t = \sim 250 \mu\text{s}$.

From the contours of e_{xx} , it can be observed that e_{xx} exhibited a positive value (tensile) directly behind the front face and a negative value (compressive) directly in front of the back face. This means that the core directly behind the front face was under tensile loading, while the core directly in front of the back face was under compressive loading. Since the shock wave loading is a compressive loading, the tensile loading in the core must be related to the wave propagation and reflection, or the fluid-structure interaction process.

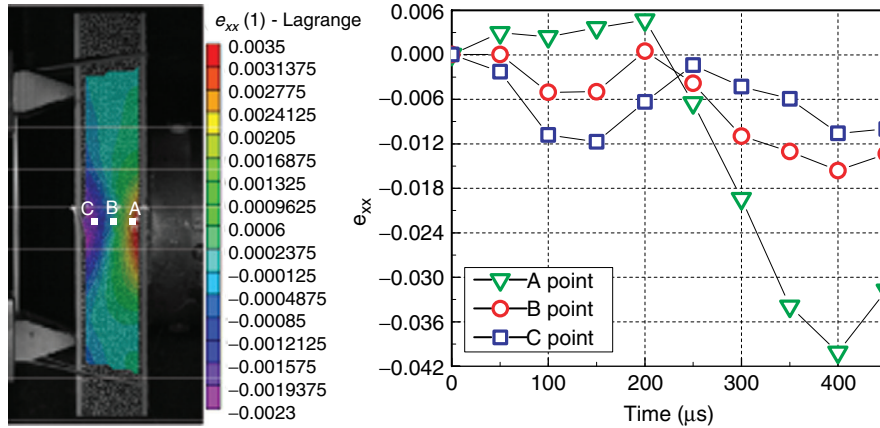


Figure 7 Transverse strain e_{xx} on the symmetric center line of core.

The 2-D DIC analysis can also be used to analyze the core shear crack initiation/formation. Figure 8 shows the contour history of the strains e_{xx} , e_{yy} , e_{xy} obtained from the 2-D DIC system. During the core crack initiation, only the shear strains e_{xy} were concentrated around the path of the core crack, which indicated that the shear strains caused the core cracks to form. Unlike the shear strains, e_{xy} , the axial strains, e_{xx} and e_{yy} , were not concentrated along the path of the core crack and had relatively small values. Figure 9 shows the history of e_{xx} , e_{yy} , and e_{xy} at the crack location. It can be observed that when the crack was opening, e_{xx} and e_{yy} were approximately 1%, while e_{xy} was around 5%. This indicated that the shear strains were the dominating factors which ultimately lead to the core cracking.

4.2.2. Real-time back-face deflection contours

The characteristic fluid-structure interaction time can also be determined using the real-time back-face deflection contours, as generated using 3-D Digital Image Correlation (DIC). A view of the back face of the specimen is shown in Figure 10. The yellow color is the original color of the specimen, while the white background and black dots are the painted speckle pattern, and subsequent viewing area used in the DIC system. The two white lines represent the simply-supported knife edge positions. The red circle represents the inner diameter of the shock tube muzzle, i.e. the loading area on the specimen.

A series of deflection contours of the back face for the different material systems are shown in Figure 11. Since the characteristic fluid-structure interaction time has been determined for the EVE sandwich composite with the 38.1 mm core in Section 4.2.1, using 2-D DIC and core deformation analysis, the back-face deflection contours for this configuration will be investigated first (Fig. 11d). It can be observed that the contours begin as a circle ($t = 100 \mu\text{s}$), which corresponds to the shock wave loading area. Then, the contours stretch and propagate towards the boundary ($t = 150 \mu\text{s}$). Finally, as the specimen deforms, these contours become parallel to the support lines ($t = 250 \mu\text{s}$). Therefore, by $t = 250 \mu\text{s}$, the wave propagation, reflection and averaging within the specimen has balanced, and initial interactions have now become a global response, i.e. the initial fluid-structure interaction was completed.

There is excellent agreement between using the real-time back-face 3-D DIC deflection contours and the 2-D DIC core deformation to determine the characteristic fluid-structure interaction time for the EVE sandwich composite with the 38.1 mm core. Consequently, this

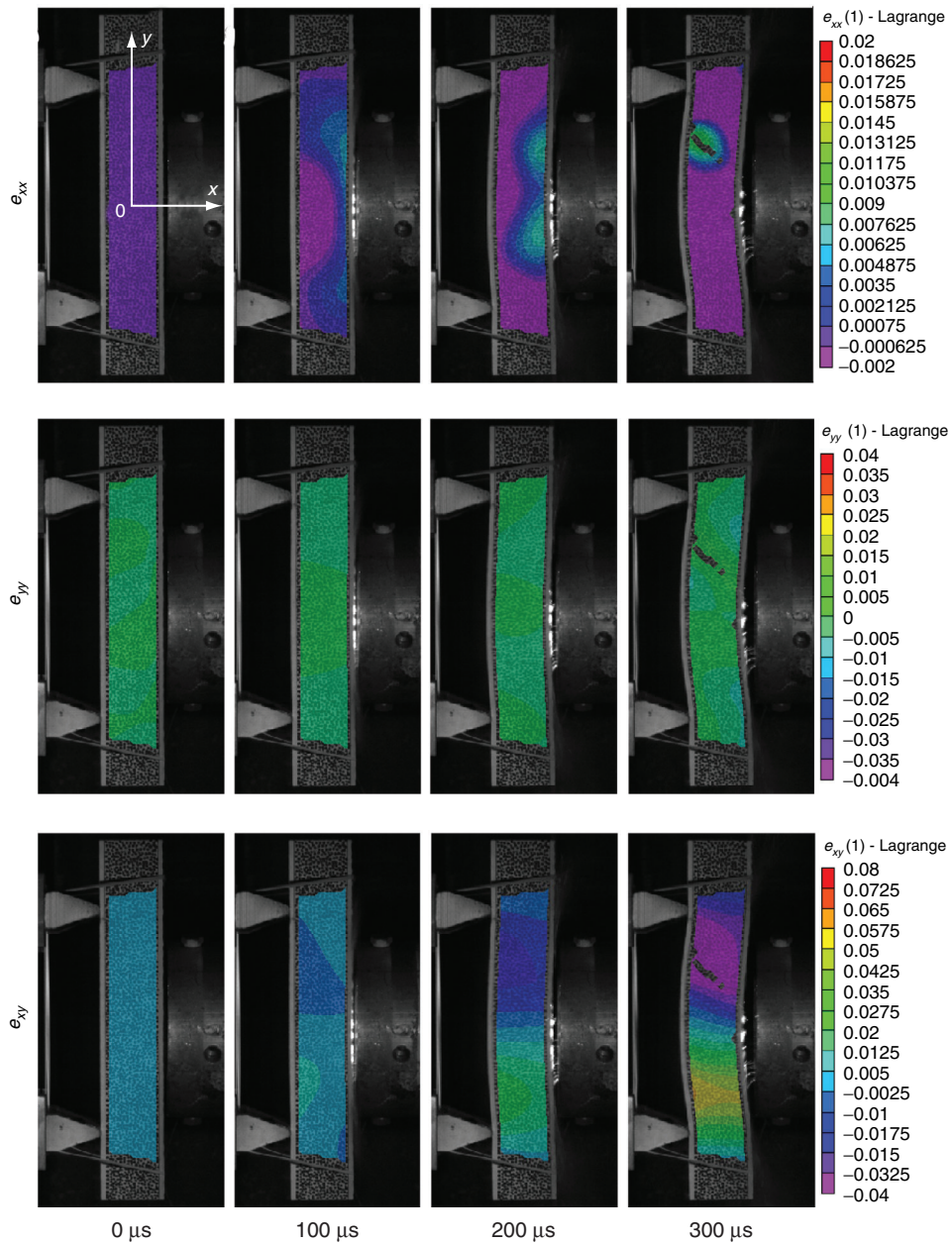


Figure 8 Comparison of strain in the core: e_{xx} , e_{yy} and e_{xy} .

method can be extended to the other material systems used, i.e. the Aluminum 6061-T6 alloy plates (Figure 11a), the EVE composite (Figure 11b) and the EVE sandwich composite with 25.4 mm core (Figure 11c). It can be observed from Figure 11, that the back face deflection contours for each material system investigated exhibit a similar trend. These contours begin as a circle corresponding to the loading area, stretch and propagate towards the boundaries, and finally become parallel to the support lines. Note, since the interframe times vary, the values of the characteristic fluid-interaction time estimated had a maximum error between 7.5% and 20%.

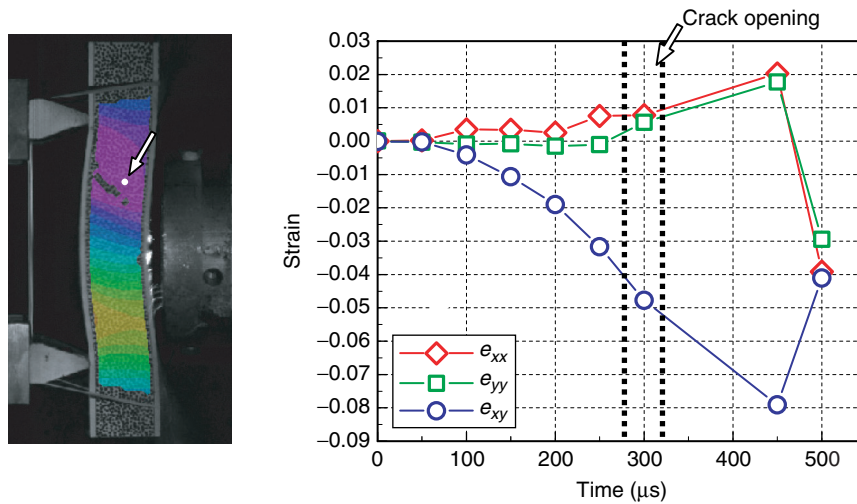


Figure 9 e_{xx} , e_{yy} and e_{xy} at the crack location of the core.

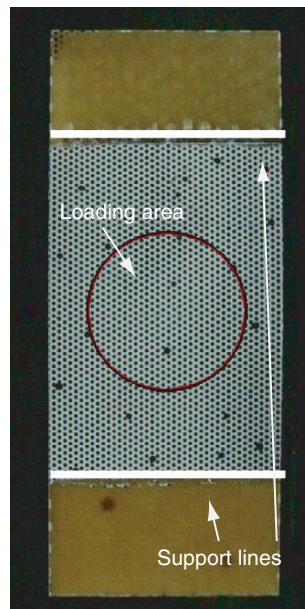


Figure 10 Back view of the specimen.

For the homogenous material system, i.e. the Aluminum 6061-T6 alloy plates (Figure 11a), the characteristic fluid-structure interaction was completed by $t = \sim 150 \mu\text{s}$. For the non-homogeneous material systems, i.e. EVE composites and sandwich structures, the characteristic fluid-structure interaction took a longer duration to complete, approximately $100 \mu\text{s}$ longer than the homogeneous material system. For the EVE composite (Figure 11b), the characteristic fluid-structure interaction was completed by $t = \sim 260 \mu\text{s}$. For both of the EVE sandwich composite systems, as shown in Figure 11c and 11d, the characteristic

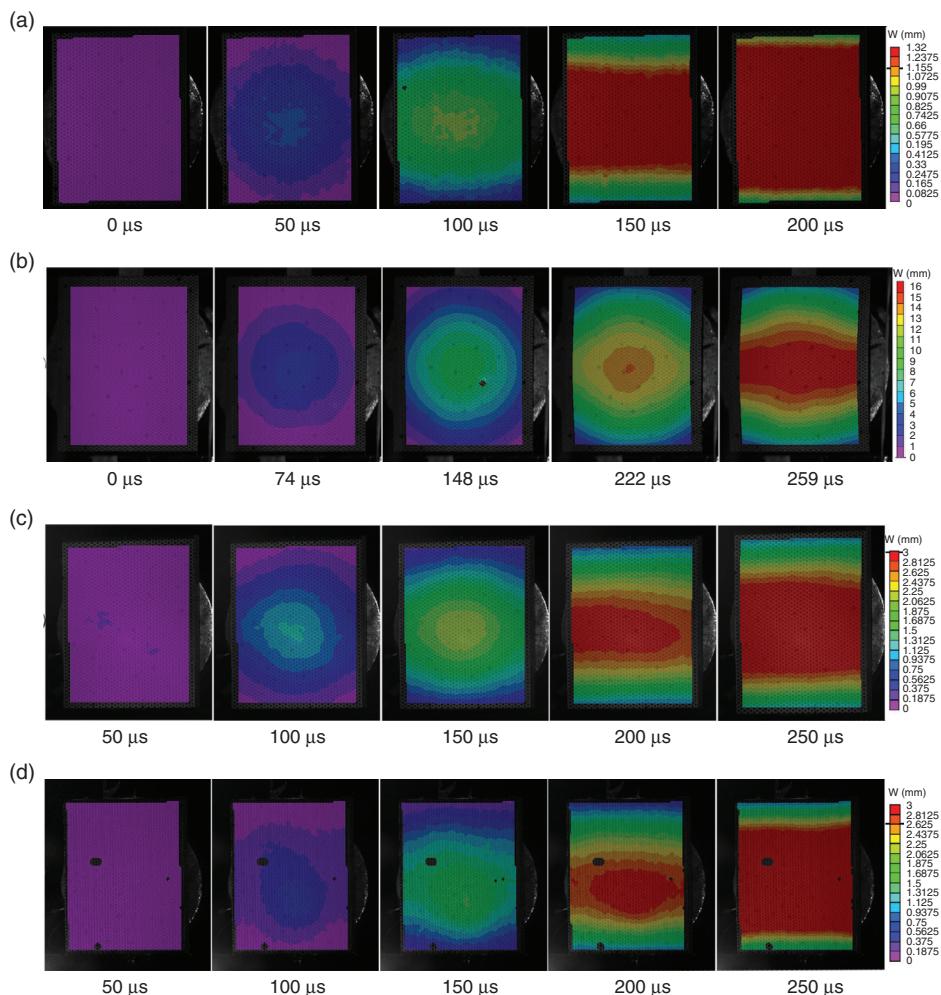


Figure 11 Back face deflection contour (a) Al alloy plate; (b) EVE composite; (c) Sandwich composite with 25.4 mm core (d) Sandwich composite with 38.1 mm core.

fluid-structure interaction was completed by $t = \sim 250 \mu\text{s}$. Therefore, the value of the characteristic fluid-structure interaction time can be directly correlated with the type of material system used (homogeneous vs. non-homogeneous). Due to the varying material properties within the non-homogeneous material systems, the characteristic fluid-structure interaction took a longer duration to complete.

One more feature that can be observed is that for the monolithic materials such as EVE composites and Aluminum alloy plates, the initial contours are all perfect circles, which correlate to the loading area (muzzle diameter). For the sandwich composites, the initial contours still exhibit a shape similar to a circle, but the center of the circle is off-center in regards to the loading area. This indicates two things; (1) the sandwich composites disperse the loading due to the soft core materials, and (2) the thickness of the core affects the amount of dispersion and shape of contour.

4.3. REAL-TIME SIDE-VIEW DEFORMATION IMAGES AND DEFLECTIONS

Based upon the time frames (images) used to define the characteristic fluid-structure interaction time in Fig. 11, the corresponding side-view deformation images are shown in Figure 12. The deflections are very small in comparison to the dimensions of the specimens.

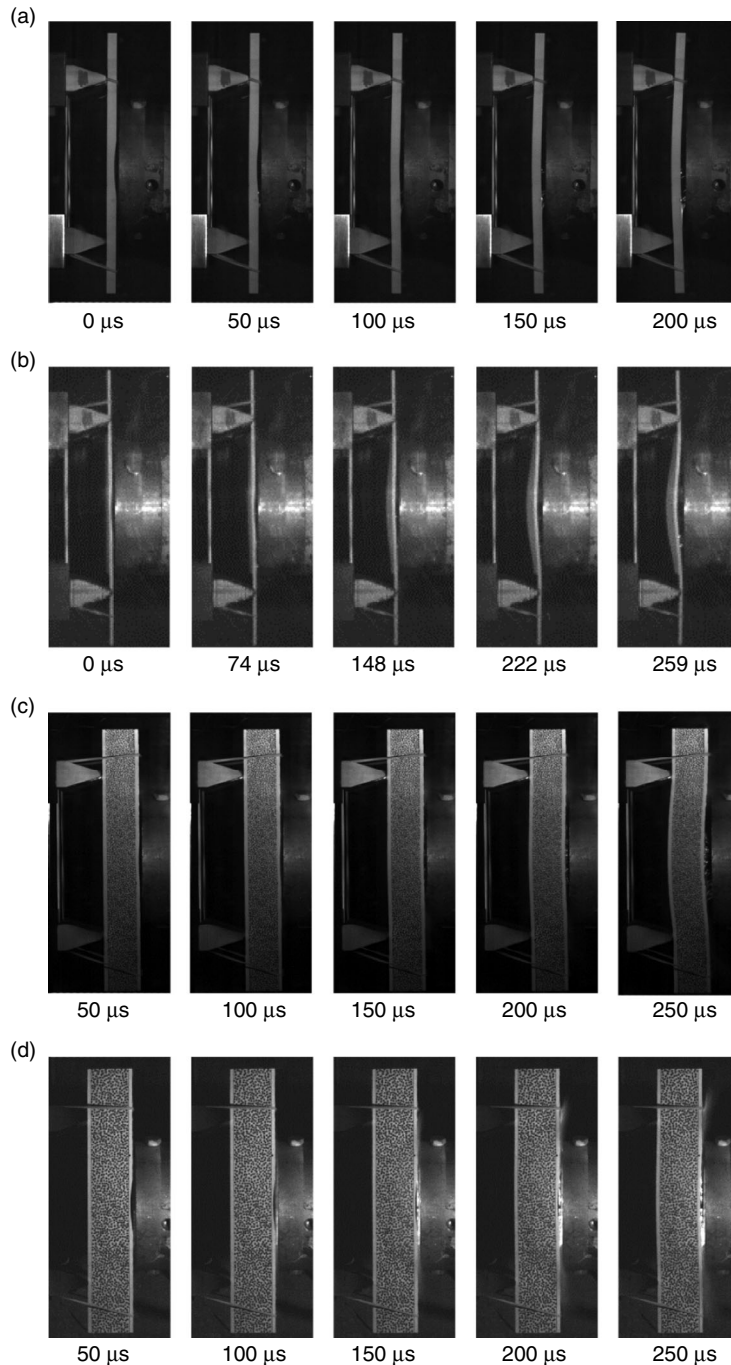


Figure 12 Side-view deformation (a) Al alloy plate; (b) EVE composite; (c) Sandwich composite with 25.4 mm core (d) Sandwich composite with 38.1 mm core.

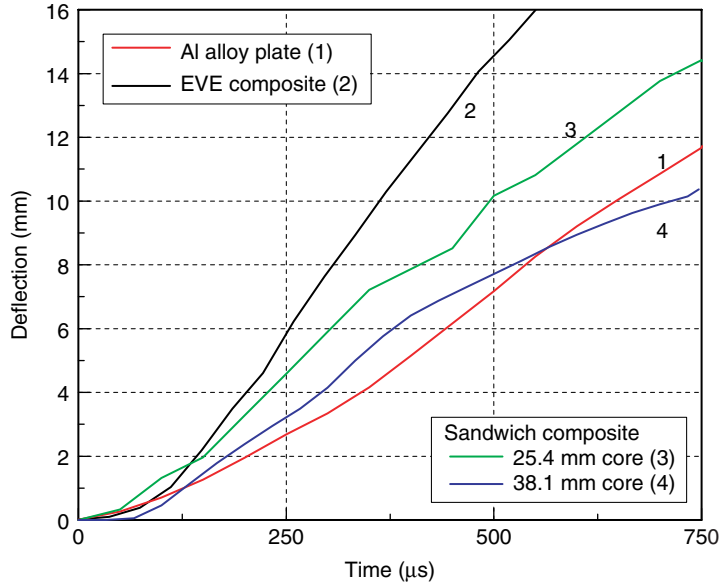
Due to the low flexural stiffness of the EVE composites, the specimens exhibit a clear 3-D deformation during the fluid-structure interaction (Figure 12b). This indicates that the supports have a minimal effect on the deformation behavior of the specimens. Even though the other materials (Aluminum plate and sandwich composites) deform in a manner similar to 2-D deformation (three point bending) during the fluid-structure interaction, they actually deform in a 3-D manner analogous to the deformation pattern of the EVE composite. This can be proven using the displacement contours shown in Figure 11, and the discussion in Section 4.2.2. As stated in the previous section, the back-face deflection contours begin as a circle corresponding to the loading area, stretch and propagate towards the boundaries, and finally become parallel to the support lines. During the initial deformation and subsequent early time frames, this circular out-of-plane deformation contour, exhibiting various amounts of deflection, shows the 3-D deformation and subsequent “punching” effect.

The deflection and velocity of the center point of the back face are shown in Figure 13a and Figure 13b respectively. During the initial fluid-structure interaction behavior, the deflections decrease as the areal density of the specimens increase, which is similar to the trend observed in the reflected pressure profiles in Figure 5. However, the deflection of the monolithic materials, such as the EVE composite and Aluminum plate, increases faster with respect to the time (accelerates), while those of the sandwich composites show a decelerating trend. This indicates that during the later global deformation process, the sandwich composites contain more mechanisms to dissipate energy, and consequently gain less kinetic energy. Therefore, it can be concluded that the overall properties of the sandwich structure play a crucial role during the fluid-structure interaction process.

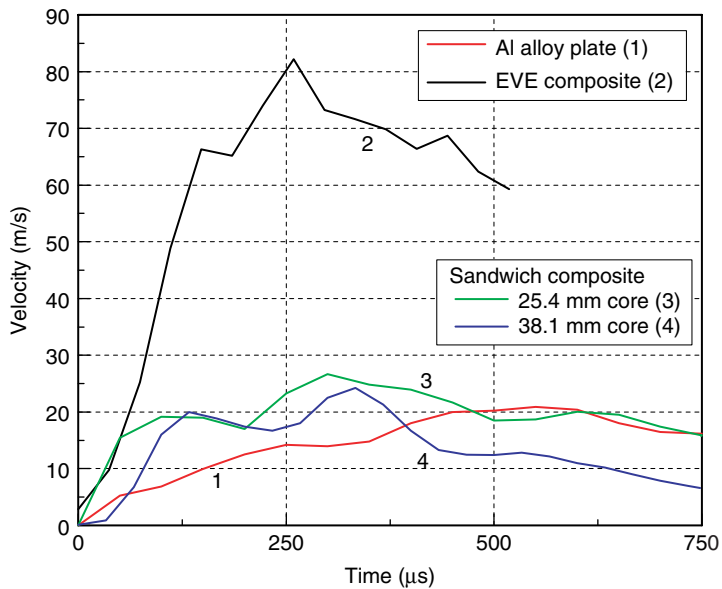
4.4. THEORETICAL PREDICTION

The predicted reflected pressure profiles, as obtained using Taylor’s model and the model by Wang *et al.* in section 2, are shown in Figure 14. Since the two models can only predict the behavior of the free-standing specimen, the simply supported boundary conditions are completely ignored. Therefore, the results are only valid during the characteristic fluid-structure interaction time, in which the simply supported boundary conditions have not affected the dynamic behaviors of the specimens. The results in Figure 14 validate the above assumption. It can clearly be seen that during the characteristic fluid-structure interaction time ($\sim 250 \mu\text{s}$), the predictions from the model by Wang *et al.*, which considers the compressibility of the gas, agrees well with the experimental results. The predictions even agree with the experimental results through $t = 500 \mu\text{s}$. After this time, the predictions drift off the experimental data, which shows the boundary condition effects on the results. Unlike the model by Wang *et al.*, Taylor’s model does not consider the compressibility of the gas and thus the theoretical predictions exhibit a large deviation from the experimental results. This reveals that Taylor’s model cannot be used in a highly compressible fluid, such as air.

For sandwich composites under blast loading, many researchers [2, 14] assumed that the fluid-structure interaction only occurs between the fluid and the facesheet which contacts the fluid, and it is independent of the core material and core thickness. Further numerical studies [10] show that the fluid-structure interaction behavior of sandwich composites lies between the following results; only considering the facesheet, and considering the sandwich composite as an equivalent monolithic plate with same areal density. Our results provide a much clearer and more comprehensive understanding of the fluid-structure interaction in sandwich composites. The experimental results and theoretical predictions of the sandwich composites and the facesheets (EVE composites) are plotted in Figure 14. For the theoretical prediction, the sandwich composite is considered to be an equivalent monolithic plate. It can be clearly seen that the fluid-structure interaction between the fluid and the sandwich composites is completely different than the fluid-structure interaction between the fluid and



(a) Back-face deflection (center-point)



(b) Back-face velocity (center-point)

Figure 13 Deflection and velocity of the back face (center-line).

the facesheet. Using the prediction of the facesheet will induce significant error. Furthermore, sandwich composites which have a core of identical material but different thicknesses, exhibit different responses from the very beginning. This indicates that the core material affects the fluid-structure interaction. These results indicate that using the model by

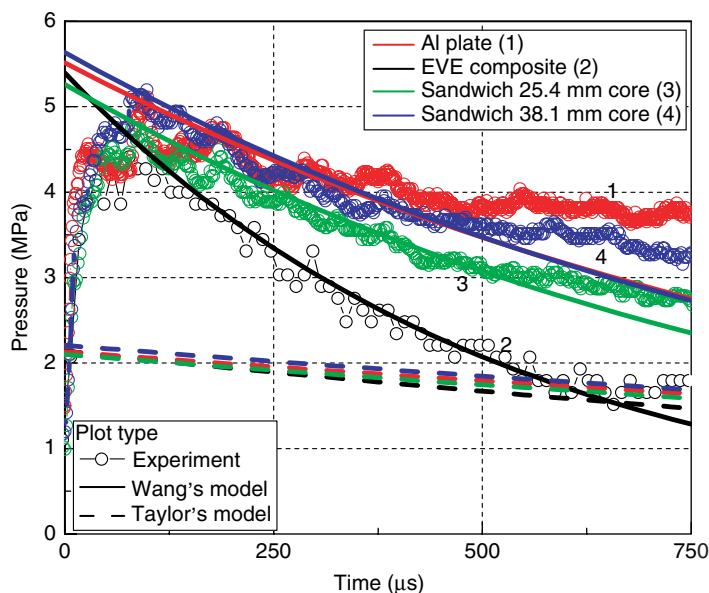


Figure 14 The comparison of theoretical and experimental reflected pressure profiles.

Wang *et al.*, and assuming the sandwich composite to be an equivalent monolithic plate with same areal density, allows for a close prediction of the reflected pressure profiles during the characteristic fluid-structure interaction time. As discussed in section 4.4, the complicated deformation and failure mechanisms will only occur and affect the results after 500 μs .

5. CONCLUSIONS

In this paper, E-glass Vinyl-Ester (EVE) composites, sandwich composites with EVE facesheet and monolithic foam core (2 different core thicknesses), and monolithic aluminum alloy plates, were subjected to shock wave loading to investigate their blast response and fluid-structure interaction behavior. The following is a summary of the investigation:

- 1) The comparison between the experimental results and predicted results from Taylor's model and the model by Wang *et al.* revealed two things; (1) The model by Wang *et al.* can provide a more accurate prediction during the characteristic fluid-structure interaction time, and (2) Taylor's model cannot be used in air due to its high compressibility.
- 2) The deflection results obtained from the 3-D Digital Image Correlation (DIC) technique showed that different material systems (homogeneous vs non-homogeneous) have different characteristic fluid-structure interaction times.
- 3) The decaying speed of the reflected pressure profiles showed a decreasing trend with increasing areal density.
- 4) The results for sandwich composites and their facesheet showed that the fluid-structure interaction between the fluid and sandwich composites cannot be simplified as the fluid-structure interaction between the fluid and the facesheet. Also, the results indicated that the core thickness affects the fluid-structure interaction behavior of sandwich composites (allows for shockwave dispersion).

ACKNOWLEDGEMENT

The authors kindly acknowledge the financial support of the Office of Naval Research (Dr. Y.D.S. Rajapakse) under grant no. N00014-10-1-0662, and the Department of Homeland Security under Cooperative Agreement No. 2008-ST-061-ED0002.

REFERENCES

- [1] Dharmasena KP, Wadley HNG, Xue Z, Hutchinson JW (2008) Mechanical response of metallic honeycomb sandwich panel structures to high-intensity dynamic loading. *International Journal of Impact Engineering* 35 (9): 1063–1074.
- [2] Fleck NA, Deshpande VS (2004) The Resistance of Clamped Sandwich Beams to Shock Loading. *Journal of Applied Mechanics* 71 (3): 386–401.
- [3] Gardner N, Wang E, Kumar P, Shukla A (2012) Blast Mitigation in a Sandwich Composite Using Graded Core and Polyurea Interlayer. *Experimental Mechanics* 52 (2): 119–133. doi: 10.1007/s11340-011-9517-9.
- [4] Gardner N, Wang E, Shukla A (2012) Performance of functionally graded sandwich composite beams under shock wave loading. *Composite Structures* 94 (5): 1755–1770.
- [5] Gupta S, Shukla A Blast Performance of Marine Foam Core Sandwich Composites at Extreme Temperatures. *Experimental Mechanics*:1–14. doi:10.1007/s11340-012-9610-8.
- [6] LeBlanc J, Shukla A (2011) Dynamic response of curved composite panels to underwater explosive loading: Experimental and computational comparisons. *Composite Structures* 93 (11): 3072–3081.
- [7] Rajamani A, Prabhakaran R (1980) Response of composite plates to blast loading. *Experimental Mechanics* 20 (7): 245–250. doi: 10.1007/bf02327708.
- [8] Wang E, Gardner N, Shukla A (2009) The blast resistance of sandwich composites with stepwise graded cores. *International Journal of Solids and Structures* 46 (18–19): 3492–3502.
- [9] KazancÄ± Z, MecitoÄlu Z (2008) Nonlinear dynamic behavior of simply supported laminated composite plates subjected to blast load. *Journal of Sound and Vibration* 317 (3–5): 883–897.
- [10] Li R, Kardomateas GA, Simitse GJ (2009) Point-wise impulse (blast) response of a composite sandwich plate including core compressibility effects. *International Journal of Solids and Structures* 46 (10): 2216–2223.
- [11] LeBlanc J, Shukla A (2011) Response of E-glass/vinyl ester composite panels to underwater explosive loading: Effects of laminate modifications. *International Journal of Impact Engineering* 38 (10): 796–803.
- [12] Motley MR, Young YL, Liu Z (2011) Three-Dimensional Underwater Shock Response of Composite Marine Structures. *Journal of Applied Mechanics* 78 (6): 061013–061010.
- [13] Wang E, Wright J, Shukla A Analytical and experimental study on the fluid structure interaction during air blast loading. *Journal of Applied Physics* 110 (11): 114901–114912.
- [14] Xue Z, Hutchinson JW (2004) A comparative study of impulse-resistant metal sandwich plates. *International Journal of Impact Engineering* 30 (10): 1283–1305.
- [15] Taylor GI (1963) pressure and impulse of submarine explosion waves on plates. In: Batchelor GK, Editor, *The Scientific Papers of Sir Geoffrey Ingram Taylor. Aerodynamics and the mechanics of Projectiles and Explosions*, Cambridge University Press 3: 287–303.
- [16] Tan PJ, Reid SR, Harrigan JJ (2005) Discussion: “The Resistance of Clamped Sandwich Beams to Shock Loading” (Fleck, N. A., and Deshpande, V. S., 2004, *ASME J. Appl. Mech.*, [bold 71], pp. 386–401). *Journal of Applied Mechanics* 72 (6): 978–979.

- [17] Karagiozova D, Langdon GS, Nurick GN, Chung Kim Yuen S (2010) Simulation of the response of fibre-metal laminates to localised blast loading. *International Journal of Impact Engineering* 37 (6): 766–782.
- [18] Kumar P, LeBlanc J, Stargel DS, Shukla A Effect of plate curvature on blast response of aluminum panels. *International Journal of Impact Engineering* 46 (0): 74–85.
- [19] Baker WE, Cox PA, Westine PS, Kulesz JJ, Strehlow RA (1983) *Explosion hazards and evaluation*. Elsevier Scientific Publishing Company.
- [20] Glasstone S (1964) *The effects of nuclear weapons*. United States Atomic Energy Commission.
- [21] Smith PD, Hetherington JG (1994) *Blast and ballistic loading of structures*. Butterworth-Heinemann, Elsevier Science Ltd.
- [22] <http://www.gurit.com> (Accessed May 15, 2012).
- [23] Wang E, Shukla A (2010) Analytical and experimental evaluation of energies during shock wave loading. *International Journal of Impact Engineering* 37 (12): 1188–1196.
- [24] Tiwari V, Sutton M, McNeill S (2007) Assessment of High Speed Imaging Systems for 2D and 3D Deformation Measurements: Methodology Development and Validation. *Experimental Mechanics* 47 (4): 561–579. doi: 10.1007/s11340-006-9011-y.
- [25] Tiwari V, Sutton MA, McNeill SR, Xu S, Deng X, Fourney WL, Bretall D (2009) Application of 3D image correlation for full-field transient plate deformation measurements during blast loading. *International Journal of Impact Engineering* 36 (6): 862–874.

